Circular Dichroism in the Angle-Resolved Photoemission Spectrum of the High-Temperature $Bi_2Sr_2CaCu_2O_{8+\delta}$ Superconductor: Can These Measurements Be Interpreted as Evidence for Time-Reversal Symmetry Breaking?

V. Arpiainen,[1] A. Bansil,[2] and M. Lindroos[1,2]

[1]*Department of Physics, Tampere University of Technology, P.O. Box 692, FIN-33101 Tampere, Finland*

[2]*Department of Physics, Northeastern University, Boston, Massachusetts 02115, USA*

(Received 18 November 2008; published 5 August 2009)

We report first-principles computations of the angle-resolved photoemission response with circularly polarized light in $Bi_2Sr_2CaCu_2O_{8+\delta}$ for the purpose of delineating contributions to the circular dichroism resulting from distortions and modulations of the crystal lattice. Comparison with available experimental results shows that the measured circular dichroism from antinodal mirror planes is reproduced in quantitative detail in calculations employing the average orthorhombic crystal structure. We thus conclude that the existing angle-resolved photoemission measurements can be understood essentially within the framework of the conventional picture, without the need to invoke unconventional mechanisms.

DOI: 10.1103/PhysRevLett.103.067005 PACS numbers: 74.72.Hs, 74.25.Jb, 74.62.Bf, 79.60.−i

A key to understanding the mechanism of superconductivity in cuprates is to unravel the nature of the pseudogap phase, which arises as a precursor to the superconducting phase when the insulator is doped with holes. A number of theoretical models of the pseudogap phase invoke the presence of circulating currents (CCs) in various configurations with breaking of the time-reversal symmetry (TRS) as one of their hallmarks [1–4]. In this connection, Varma [5,6] has proposed that the breaking of TRS could be tested by using circularly polarized light in angle-resolved photoemission (ARPES) experiments. Specifically, the observation of a nonzero circular dichroism signal from a symmetry plane of the sample, i.e., the difference between the ARPES intensities for left-handed (LH) and right-handed (RH) polarized light, would provide evidence for the existence of the CCs. Kaminski *et al.* [7] carried out ARPES experiments on a thin Bi2212 film and reported support for TRS breaking. This conclusion, however, has been challenged by others, implicating possible dichroic effects resulting from the breaking of reflection symmetry due to temperature-dependent changes in the geometry of the lattice [8] or from the presence of superstructure in Bi2212 [9–11]. Here we report first-principles computations, which include the effects of the ARPES matrix element [18] and allow us to assess quantitatively how distortions of the lattice contribute to a dichroic signal in Bi2212. We find that the existing ARPES measurements can be understood essentially within the conventional picture without the need to invoke unconventional mechanisms.

Our focus is on calculating the dichroic effect in distorted geometry using the correct crystal symmetry. Specifically, we use an average of the incommensurate structure [19] represented by an orthorhombic unit cell, i.e., a centrosymmetric bbmb structure, refined using neutron spectroscopy by Miles *et al.* [20] at 12 K for an optimally doped single crystal sample. This structure is consistent with ARPES studies which show the presence of both a mirror and a glide plane in Bi2212 [21]. In the orthorhombic distortion, the atoms in the Cu-O layer almost maintain their symmetric positions, but the Bi-O layer is distorted. The states forming the Fermi surface originate in the Cu-O layer, and distortions in that layer would change the band dispersions strongly. In contrast, distortions in the Bi-O layer have little effect on the Fermi surface, but the effect on ARPES intensities is substantial. To our knowledge there are no quantitative refinements of the surface reconstruction, and for this reason a cleavage surface terminated at the Bi-O layer is used in the present calculations, without allowing for possible surface reconstructions or relaxations.

The details of our one-step approach to photoemission are given elsewhere [22–24]. The imaginary parts of the initial and final state self-energies were chosen to be 0.1 and 2 eV, respectively, since these values have been shown to yield a good level of agreement between calculations and measurements in our recent studies [24]. In any event, normalized circular dichroism D_n, which is our main concern in this study, is insensitive to the choice of these parameters. We define D_n by

$$D_n = \frac{I_{\mathrm{LH}} - I_{\mathrm{RH}}}{I_{\mathrm{LH}} + I_{\mathrm{RH}}} = \frac{D}{I_{\mathrm{LH}} + I_{\mathrm{RH}}}, \tag{1}$$

where $D = I_{\mathrm{LH}} - I_{\mathrm{RH}}$ denotes the intensity of the dichroic signal.

The theoretical dichroic signal in orthorhombic Bi2212 is considered in Fig. 1 using 21 eV light incident normally to the surface. The computed intensities for LH- and RH polarized light are shown in Figs. 1(a) and 1(b), respectively. These maps may be thought of as a representation of the Fermi surface as seen in photoemission. The key, however, is the dichroic signal D shown in Fig. 1(c), obtained by taking the difference of the maps in Figs. 1(a) and 1(b). Note that there are two symmetry planes relevant for photoemission spectroscopy in the structure: a mirror plane

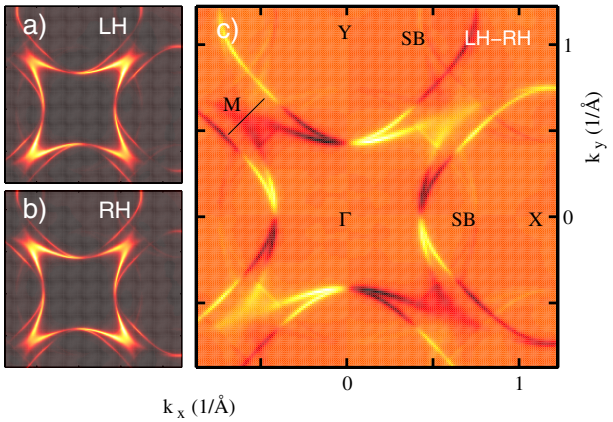

FIG. 1 (color online). Theoretically obtained photointensity in orthorhombic Bi2212 for emission from the Fermi energy using 21 eV light incident normally to the surface. (a) LH polarized light; (b) RH polarized light; and (c) dichroic intensity obtained by taking the difference (LH-RH) of the maps in (a) and (b). Black denotes low and white denotes high intensity.

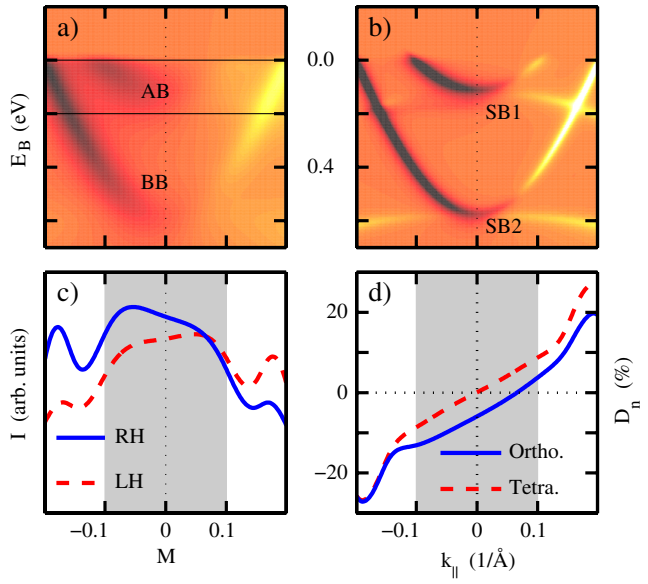

FIG. 2 (color online). Computed dichroic intensity at and near the $M(\pi, 0)$ symmetry point. (a) Dichroic intensity as a function of binding energy for momenta along the black line in Fig. 1(c). The horizontal axis denotes $k_\parallel$ distance from the M point, where $\mathbf{k}_\parallel = 0$ is the M point. (b) The same as (a), except this panel corresponds to a very small initial state width to highlight various spectral features (AB, BB, SB) discussed in the text. (c) Spectral weight integrated over the binding energy range of 0–0.2 eV [pair of black horizontal lines in (a)] for RH and LH polarized light. (d) Normalized dichroic signal D_n, energy-integrated over the 0–0.2 eV binding energy range, for the orthorhombic and tetragonal structures.

parallel to the y axis and a glide plane parallel to the x axis. Since D is antisymmetric with respect to reflections at symmetry planes of the sample [24], D is exactly zero at these planes which lie along the $\Gamma - X$ and $\Gamma - Y$ directions. The mirror planes parallel to the Cu-O bonds, corresponding to directions $\Gamma - M$, are lost, and so is the fourfold rotation symmetry in Figs. 1(a) and 1(b). The faint shadow bands [marked SB in Fig. 1(c)] result from the doubling of the unit cell in going from the tetragonal to the orthorhombic structure [21,25].

We now turn to address the dichroism of the spectra at a quantitative level. In this connection, Fig. 2(a) shows how the dichroic intensity varies in the vicinity of the M symmetry point as a function of energy for momenta $\mathbf{k}_\parallel$ lying along the black line in Fig. 1(c). The same spectrum is plotted in Fig. 2(b) using a very small initial state linewidth of 0.02 eV to better reveal various bands underlying the spectrum. For example, the shadow bands (SB1 and SB2) around binding energies of 0.2 and 0.6 eV are seen more clearly in Fig. 2(b), in addition to the familiar bonding (BB) and antibonding (AB) bands. For comparing dichroic intensity with experiments, a convenient measure is to consider the integrated spectral weight between the binding energy window of 0–0.2 eV [pair of black horizontal lines in Fig. 2(a)] because in this way one can isolate the contribution of just the AB band close to the M point. The integrated weights so obtained as a function of $\mathbf{k}_\parallel$ in a narrow momentum range around M are given in Figs. 2(c) and 2(d). [Here $\mathbf{k}_\parallel = 0$ denotes the M point.] Figure 2(c) shows how these weights vary with $\mathbf{k}_\parallel$ for the LH and RH polarized light; the bumps in Fig. 2(c) for $\mathbf{k}_\parallel < -0.1$ and for $\mathbf{k}_\parallel > 0.1$ arise because at these momenta the BB band begins to contribute. For this reason, only the $\mathbf{k}_\parallel$ range of -0.1 to $+0.1$ shown by gray shading in Figs. 2(c) and 2(d) is most relevant for discussing the dichroic signal of the AB band. With this background, Fig. 2(d) compares the normalized, energy-integrated dichroic weight D_n of Eq. (1) in the tetragonal (dashed red line) and orthorhombic (solid blue line) structures. D_n is seen to vary essentially linearly in the narrow shaded $\mathbf{k}_\parallel$ range for both structures, but as expected, for the tetragonal case, $D_n = 0$ at the M point due to symmetry of the lattice. The orthorhombic distortion breaks the symmetry of the mirror plane through the M point, and the resulting dichroic signal is quite substantial, amounting to about 6% in Fig. 2(d) at the M point.

Note that near the M point, in principle, the integrated weights D_n of Fig. 2(d) for the orthorhombic case include the contribution of the shadow band SB1 in addition to that of the main antibonding band AB. We see from Fig. 2(b), however, that the spectral weight of SB1 close to the M point is small, and, therefore, the dichroic response at M is dominated by the antibonding band. Interestingly, Refs. [9,26] have suggested that the umklapp bands or the diffraction replicas of the main bands resulting from the presence of the superstructure in Bi2212 are important in explaining the observed dichroic effects in the ARPES spectra. Our calculations, on the other hand, indicate that extra bands such as the shadow and umklapp bands do not play a significant role in the symmetry breaking dichroic signal.

Figure 3 provides further insight into how the dichroic response D_n at the M point evolves with geometric distortion by considering a series of geometries starting with the tetragonal structure, which is then distorted gradually into the orthorhombic low-T structure of Ref. [20] by varying all of the atomic positions uniformly. The dichroic response is seen to depend quite strongly on the excitation energy. At 25 eV, the response varies quadratically with the degree of distortion reaching -13.6% for the fully distorted geometry. The behavior at 50 eV is almost a mirror replica of that at 25 eV. At 21 eV, the response is much smaller, being quadratic only for small distortions and then becoming linear with a maximum of about -6%. At 30 eV, the response rises slightly at small distortions but falls back to becoming essentially zero by 50% distortion, rising again slowly to a value of 2.5% at the 100% distortion. These results establish very clearly that the size of the dichroic signal can vary anywhere from -15% to 15% in Bi2212 depending on the degree of orthorhombic distortion and the choice of the excitation energy.

We delineate temperature effects on the dichroic signal with reference to Fig. 4 on the basis of the structural refinements of Miles *et al.* [20] at 12 K and room temperature. Insofar as dichroic effects are concerned, the key structural change involves the movement of the y coordinate of the O atoms in the Bi-O layer in that these atoms move by 0.05 Å closer to the tetragonal position when the temperature is raised from 12 to 298 K. In this connection, Fig. 4(a) shows how the energy-integrated intensity for the LH and RH polarized light varies with momentum in a narrow momentum range around the M point at 12 and 298 K for 21 eV photons. (The horizontal scale here has been chosen to be the same as that used in Figs. 3 and 4 of Ref. [7].) For both the LH and the RH polarized light, the reduced distortion of the tetragonal structure at the higher temperature is seen to induce a reduction in intensity. The corresponding dichroic signal in Fig. 4(b) also shows a momentum-dependent reduction of a few percent in the value of D_n at the M point, which is in agreement with the experimental results of Ref. [7]. Moreover, the computed dichroism is odd with respect to rotating the sample by 90°, which is also in accord with the experimental observations of Ref. [7].

Table I provides a comprehensive comparison between our low- and room-temperature predictions with the available experimental data. Experimental results include room-temperature measurements of Borisenko *et al.* [9] on a single crystal sample of Bi2212 with O and Pb doping and those of Kaminski *et al.* [7] on a thin-film sample at low and room temperature. Computed values of the energy-integrated dichroic intensity D_n are given at three different excitation energies $h\nu$. Considering the single crystal data of Ref. [9] in the first experimental column, the measured D_n value of 5% at room temperature is seen to be in excellent accord with the corresponding computed value of 6% at 49.7 eV.

Turning to the 2nd experimental column for the thin-film data of Ref. [7], the measured change of 3% in going from the room to low temperature is in reasonable accord with the computed change of 1.5% at 21 eV in Table I. We emphasize that the value of D_n is seen from Fig. 3 to be quite sensitive to the photon energy, and it can vary anywhere from zero to 15%. But the three theory columns in Table I show very clearly that the *change* in the value of D_n is rather insensitive to photon energy and shows an increase of a few percent quite consistently in going from the room- to the low-temperature structure. The zero measured dichroic signal reported by Ref. [7] at room temperature is most likely the result of a different structure of the thin-film samples (compared to bulk single crystals of Ref. [9]), especially in the surface region which is probed preferentially by photoemission [27]. Notably, the superstructure signal was found to be very small in ARPES and x-ray

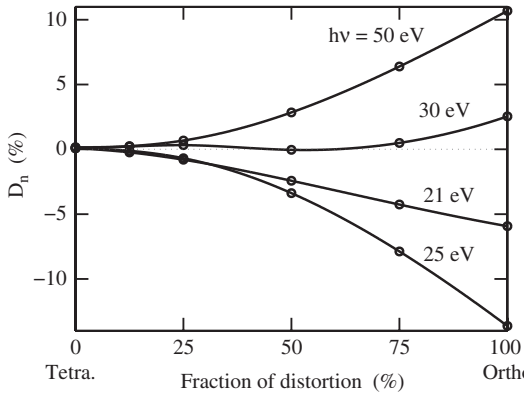

FIG. 3. Energy-integrated dichroic weight D_n at the M point as a function of geometric distortion. The horizontal axis gives the fractional (in percent) movement of the atoms in going from the tetragonal to the experimental orthorhombic structure at 12 K. Smooth lines have been drawn through the computed points.

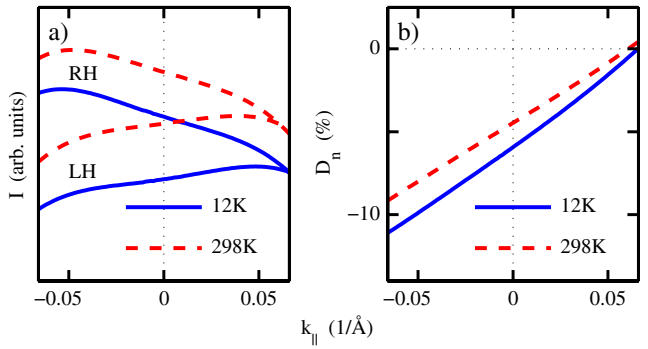

FIG. 4 (color online). (a) Computed energy-integrated intensity in Bi2212 near the M point for the experimentally refined orthorhombic structures at 12 (solid blue lines) and 298 K (dashed red lines) of Ref. [20]. The horizontal axis is the same as in Fig. 2 except for a narrower momentum range with $k_{\|} = 0$ corresponding to the M point. Results are for LH and RH polarized light at 21 eV. (b) Dichroic signal obtained by taking the difference LH-RH from the results in (a).

TABLE I. Computed values of the energy-integrated dichroic intensity D_n (in percent) at the M point for low- and room-temperature orthorhombic structure of Bi2212 at different photon energies $h\nu$ are compared with the available measurements. Experimental results are from Ref. [7] for a thin-film sample and from Ref. [9] for samples with O and Pb doping.

	Theory			Experiment		
				Single crystal [9]	Thin film [7]	Lead-doped [9]
$h\nu$ (eV)	21	30	49.7	49.7	21	49.7
D_n (%) at 298 K	4.5	1	6	5	0	0
D_n (%) at 12 K	6	2.5	9.5		3	0

scattering [7] experiments on thin-film samples, indicating structural changes in comparison to the bulk case.

Finally, we see from the 3rd experimental column in Table I that Ref. [9] found a zero dichroic signal at both room and low temperature from Pb-doped samples. These results are very consistent with the conclusions of this study that subtle movements and orderings of the atoms particularly in the surface region can lead to large changes in dichroic effects—in the case of Pb-doped samples, to an effective restoration of the mirror planes in the photoemission spectra leading to zero dichroic signal.

In conclusion, we have carried out first-principles computations of ARPES response with circularly polarized light in Bi2212 with a focus on understanding how the distortions and modulations of the crystal lattice yield circular dichroism within the conventional picture of the electronic states in this system. Comparison with available experimental results shows that the measured dichroism from antinodal mirror planes is reproduced in substantial detail in computations employing the average orthorhombic crystal structure [28]. Our study clearly establishes the sensitivity of dichroism to structural details and the viability of the geometric mechanism in explaining existing measurements and indicates that the detection of time-reversal symmetry breaking via ARPES using circularly polarized light will be complicated by the masking effects of the lattice distortions.

We thank R. S. Markiewicz for discussion and J. C. Campuzano and S. V. Borisenko for valuable information concerning their experimental work. One of us (V. A.) acknowledges Väisälä Foundation, Pirkanmaa Trust, Finnish Foundation for Technology Promotion, and Magnus Ehrnrooth Foundation for financial support. This work is supported by the U.S. DOE, Basic Energy Sciences, Division of Materials Science and Engineering Contract No. DE-FG02-07ER46352, and benefited from the allocation of time at the Institute of Advanced Computing (IAC, Tampere), Techila Technologies computational solutions, the NERSC supercomputing center, and Northeastern University's Advanced Scientific Computation Center (ASCC).

[1] I. Affleck and J. B. Marston, Phys. Rev. B **37**, 3774 (1988).
[2] S. Chakravarty *et al.*, Phys. Rev. B **63**, 094503 (2001).
[3] C. M. Varma, Phys. Rev. B **73**, 155113 (2006).
[4] P. A. Lee, N. Nagaosa, and X.-G. Wen, Rev. Mod. Phys. **78**, 17 (2006).
[5] C. M. Varma, Phys. Rev. B **61**, R3804 (2000).
[6] M. E. Simon and C. M. Varma, Phys. Rev. Lett. **89**, 247003 (2002).
[7] A. Kaminski *et al.*, Nature (London) **416**, 610 (2002).
[8] N. P. Armitage and J. Hu, Philos. Mag. Lett. **84**, 105 (2004).
[9] S. V. Borisenko *et al.*, Nature (London), doi:10.1038/nature02931 (2004).
[10] S. V. Borisenko *et al.*, Phys. Rev. Lett. **92**, 207001 (2004).
[11] Recent experiments involving neutron scattering [12,13], x-ray optical activity [14,15], the polar Kerr effect [16], and muon spin relaxation [17] have also provided controversial evidence for the CC scenarios.
[12] B. Fauqué *et al.*, Phys. Rev. Lett. **96**, 197001 (2006).
[13] Y. Li *et al.*, Nature (London) **455**, 372 (2008).
[14] M. Kubota *et al.*, J. Phys. Soc. Jpn. **75**, 053706 (2006).
[15] S. Di Matteo and M. R. Norman, Phys. Rev. B **76**, 014510 (2007).
[16] J. Xia *et al.*, Phys. Rev. Lett. **100**, 127002 (2008).
[17] G. J. MacDougall *et al.*, Phys. Rev. Lett. **101**, 017001 (2008).
[18] A. Bansil and M. Lindroos, Phys. Rev. Lett. **83**, 5154 (1999).
[19] J. P. Castellan *et al.*, Phys. Rev. B **73**, 174505 (2006).
[20] P. A. Miles *et al.*, Physica (Amsterdam) **294C**, 275 (1998).
[21] A. Mans *et al.*, Phys. Rev. Lett. **96**, 107007 (2006).
[22] J. B. Pendry, Surf. Sci. **57**, 679 (1976).
[23] M. Lindroos *et al.*, Phys. Rev. B **65**, 054514 (2002).
[24] V. Arpiainen *et al.*, Phys. Rev. B **77**, 024520 (2008).
[25] V. Arpiainen and M. Lindroos, Phys. Rev. Lett. **97**, 037601 (2006).
[26] J. C. Campuzano *et al.*, Nature (London), doi:10.1038/nature02932 (2004).
[27] There also are inherent uncertainties in the placement of the final states in first-principles computations, so that differences of a few eVs in the values of photon energy used in computations and measurements are not considered serious, but the absolute value of D_n is seen from Fig. 3 to be sensitive to photon energy and in fact is only 1% in the room-temperature computations at 30 eV in Table I.
[28] A recent analysis of the STM spectrum of Bi2212 also indicates that the characteristic asymmetry of the spectrum can be largely understood within the conventional picture [29].
[29] J. Nieminen *et al.*, Phys. Rev. Lett. **102**, 037001 (2009).